Supporting Information

A phosphorus-doped carbon material derived from sodium alginate/ phosphoric acid hydrogel as an efficient catalyst for catalytic oxidation of furfural to maleic acid

Lutong Jiao, [a,b] Chenyu Wang, [a] Yuhui Wu, [a] Han Meng, [a] Peijun Ji*[a]

[a] College of Chemical Engineering, Beijing University of Chemical Technology, Beijing 100029, PR China.

[b] School of Chemistry and Chemical Engineering, Tarim University, Alar, Xinjiang 843300, PR China.

Table S1 Comparison of the activity of various metal-free heterogeneous catalysts for the oxidation of furfural to maleic acid.

Catalyst	Reaction conditions[a]	Conv. (%)	$Yield_{MA}$ (%)	TOF[b] ($\times 10^{-3}$)	Reference
Ambelyst-70	1.8 g / 477 mM / 50 °C / 24 h	100	20	0.08	S1
Ambelyst-15	50 mg / 294 mM / 80 °C / 24 h	>99	11	0.09	S2
SO_3H/GO-HT	50 mg / 278 mM / 70 °C / 24 h	79.8	1.2	0.05	S3
Graphite	50 mg / 100 mM / 80 °C / 5 h	99	17	0.68	S4
KIT-6	60 mg/ 2000 mM / 70 °C / 1 h	46.8	2.8	0.47	S5
P-C-600	150 mg / 333 mM / 60 °C / 10 h	100	76.3	1.27	S6
NC-900	50 mg / 100 mM / 80 °C / 5 h	100	61	2.44	S4
g-C_3N_4	50 mg / 333 mM /100 °C / 3 h	>99	16.8	3.36	S7
PC-700	210 mg /1000 mM / 80 °C / 5 h	100	74.8	7.12	This work

[a] These data represent catalyst dosage, furfural concentration, reaction temperature and reaction time.

[b] Turnover frequency (TOF) = $\frac{mole\ of\ MA\ produced}{dosage\ of\ the\ catalyst\ \times reaction\ time}(mol \cdot g^{-1} \cdot h^{-1})$.

Ambelyst-70 and Ambelyst-15: solid acid catalyst (sulfonated polystyrene-based ion-exchange resin). SO_3H/GO-HT: SO_3H-modified graphite oxide reduced at high temperature. KIT-6: well-ordered mesoporous silica. PC-600: phytic acid-derived phosphorus-doped carbon catalyst. NC-900: ZIF-8-derived nitrogen-doped porous carbon. g-C_3N_4: graphitic carbon nitride.

* Corresponding author. E-mail address: jipj@buct.edu.cn

Table S2 The phosphorus content and specific surface areas of various P-doped carbon materials.

Catalyst	Precursors	Total P (wt %)[a]	Surface areas (m^2/g)	Reference
PC-700	Soluble starch and H_3PO_4	2.4	1612.9	S8
P-C-600	Phytic acid	14.1	1038.6	S6
PCF	sodium polyacrylate and hexametaphosphate	0.53	697.6	S9
P-PCN-800	Glucose and P_2O_5	2.55	1555.5	S10
PGc	Phytic acid	11	1200	S11
PMCS	Glucose and phytic acid	6.05 [b]	574.7	S12
MCel-PC-4(800)	Cellulose and H_3PO_4	6.8	641	S13
P/N-0.75	Resorcinol, F127 and H_3PO_4	6.18	94	S14
PC600	α-Cellulose and H_3PO_4	8.8 [c]	1491	S15
PG	Triphenylphosphine	4.07 [d]	1414	S16
RGO-P	Graphene Oxide and NaH_2PO_2	5.93	-	S17
PG800S	Graphene and H_3PO_4	6.89	100	S18
CFs-P15	Polyacrylonitrile and H_3PO_4	1.4 [d]	50.6	S19
PFRC500	Furfural residue and H_3PO_4	7.74	1769.4	S20
POMC	Acetylene and triphenylphosphine	0.13	403.5	S21
WAPC-4/P	Walnut shell and red phosphorus	4.88	2518.4	S22
P-C-800	Phytic acid	9.19	1464.6	S23
HPCSCMs	Cotton stalks and H_3PO_4	7.7 [b]	3463.1	S24
PBCs	Wood powder and H_3PO_4	9.83	1038.1-	S25
0.075-PC	Sucrose and H_3PO_4	4.26	802	S26
PMC	Sucrose and H_3PO_4	9.6	830	S27
ACPH800	Orange peel and H_3PO_4	0.82 [b]	1204	S28

[a] The data from XPS (wt%). [b] The data from EDS (wt%). [c] The data from X-ray fluorescence spectroscopic (XRF) (wt%). [d] The data from ICP-OES (wt%).

PC-700: starch-derived phosphorus-doped carbon materials. P-C-600: phytic acid-derived phosphorus-doped carbon materials. PCF: P-doped carbon foam. P-PCN-800: P-doped porous carbon nanosheets. PGc: P-doped graphitic carbon. PMCS: phosphorus-doped macroporous carbon spheres. MCel-PC-4(800): microcrystalline cellulose derived P-doped carbons. P/N-0.75: Phosphorylated mesoporous carbons. PC-600: cellulose-phosphoric supramolecular collosol derived P-doped carbon materials. PG: phosphorus-doped nanomesh graphene. RGO-P: amorphous phosphorus-doped graphene. PG800S: P-doped carbon materials. CFs-P15: Phosphorus-doped hard carbon nanofibers. PFRC500: P-doped furfural residue-based carbon materials. POMC: phosphorus-doped cubic ordered mesoporous carbon. WAPC-4/P: walnut shell-derived P-doped porous carbon. P-C-800: P-doped carbon. HPCSCMs: hierarchical P-doped cotton stalk carbon materials. PBCs: P-doped biochars. 0.075-PC: P-doped microporous carbon (0.075 is the phosphorus/carbon molar ratio). PMC: P-doped mesoporous carbon. ACPH800: P-doped activated carbon.

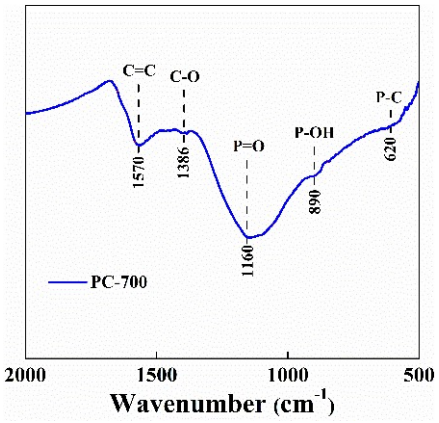

Fig. S1 FT-IR spectrum of PC-700.

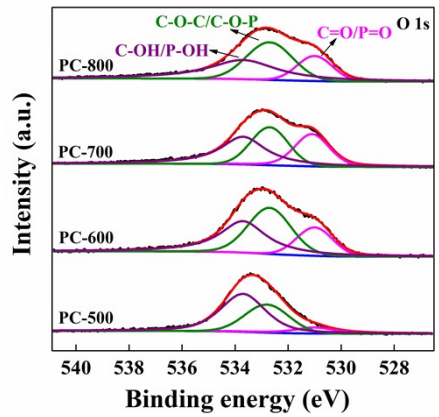

Fig. S2 The deconvolution of the O 1s peak of PC-Ts.

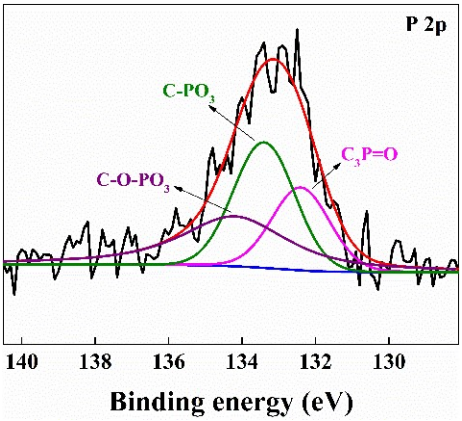

Fig. S3 The deconvolution of the P 2p peak of P&SA-700.

$$H_2O_2 \xrightarrow{\text{PC-700}} HO^{\bullet} + HO^{-} \quad \text{(SI)}$$

$$H_2O_2 \xrightarrow{\text{PC-700}} HOO^{\bullet} + H^{+} \quad \text{(SII)}$$

$$HOO^{\bullet} + HOO^{\bullet} \longrightarrow H_2O_2 + O_2 \quad \text{(SIII)}$$

$$HO^{\bullet} + \text{furfural} \longrightarrow \text{furfural radical} \longrightarrow \cdots \longrightarrow \text{maleic acid} \quad \text{(SIV)}$$

$$HO^{\bullet} + \text{maleic acid} \xrightarrow{\text{degradation}} CO_2 + H_2O \quad \text{(SV)}$$

Scheme S1 The decomposition of H_2O_2 over PC-700.

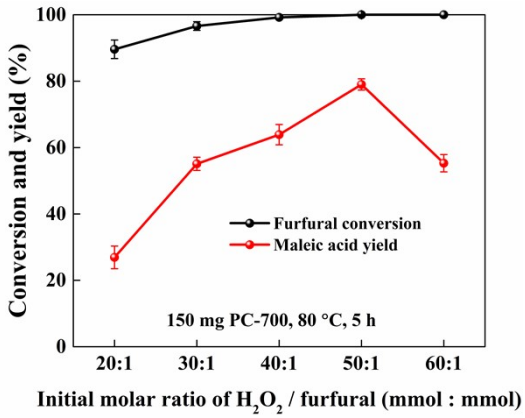

Fig. S4 The effect of initial molar ratio of H_2O_2 to furfural on the conversion of furfural and the yield of maleic acid.

Reaction conditions: 150 mg PC-700, 1 mmol furfural, 5 mL H_2O, 80 °C, 5 h, stirring rate 500 rpm.

Catalyst characterization

Scanning electron microscope (SEM, HITACHI SU8020, acceleration voltage: 15 kV) was used to observe the morphology of samples. X-ray photoelectron spectroscopy (XPS) spectra were measured using a Thermo VF ESCALAB 250Xi spectrometer. The Al Kα X-ray was used as the excitation source at the pressure of 2×10^{-8} Pa for the XPS measurement. Powder X-ray diffraction (XRD) was measured with a Rigaku-Ultima IV instrument with 2θ range from 5° to 90° and the scanning speed was 10°/min. Infrared spectra were measured with a Nicolet iS10 FT-IR spectrometer at a nominal resolution of 4 cm^{-1}. The Raman spectra were recorded with a Renishaw InVia Reflex Raman microscope with an excitation wavelength of 785 nm. The electron paramagnetic resonance (EPR) spectra were characterized using a Bruker EMX-plus spectrometer. And the 5,5-dimethyl-1-pyrroline N-oxide (DMPO) was used as spin-trapping agent. Typically, the aqueous solution of DMPO was added

to the samples, and then the mixture was transferred into an EPR tube for EPR experiments. The N_2 adsorption measurements were measured with a Micromeritics ASAP 2460 instrument at 77 K. The sample was degassed at 120 °C for 12 h before the measurement. Using the Brunauer–Emmett–Teller (BET) method, the surface area was calculated based on the adsorption isotherm data points and the pore size distribution was determined.

References

S1 N. Alonso-Fagundez, I. Agirrezabal-Telleria, P. L. Arias, J. L. G. Fierro, R. Mariscal and M. L. Granados, *RSC Adv.*, 2014, **4**, 54960-54972.

S2 H. Choudhary, S. Nishimura and K. Ebitani, *Appl. Catal., A*, 2013, **458**, 55-62.

S3 W. Z. Zhu, F. R. Tao, S. W. Chen, M. Li, Y. X. Yang and G. Q. Lv, *ACS Sustainable Chem. Eng.*, 2019, **7**, 296-305.

S4 C. V. Nguyen, J. R. Boo, C. H. Liu, T. Ahamad, S. M. Alshehri, B. M. Matsagar and K. C. W. Wu, *Catal. Sci. Technol.*, 2020, **10**, 1498-1506.

S5 M. Rezaei, A. N. Chermahini, H. A. Dabbagh, M. Saraji and A. Shahvar, *Journal of Environmental Chemical Engineering*, 2019, **7**, 102855.

S6 H. F. Zhang, S. L. Wang, H. X. Zhang, J. H. Clark and F. H. Cao, *Green Chem.*, 2021, **23**, 1370-1381.

S7 T. Yang, W. Z. Li, Q. C. Liu, M. X. Su, T. W. Zhang and J. R. Ma, *BioResources*, 2019, **14**, 5025-5044.

S8 X. Hu, M. Fan, Y. Zhu, Q. Zhu, Q. Song and Z. Dong, *Green Chem.*, 2019, **21**, 5274-5283.

S9 Y. Zou, D. Guo, B. Yang, L. Zhou, P. Lin, J. Wang, X. a. Chen and S. Wang, *ACS Appl. Mater. Interfaces*, 2021, **13**, 50093-50100.

S10 G. Zhong, S. Lei, X. Hu, Y. Ji, Y. Liu, J. Yuan, J. Li, H. Zhan and Z. Wen, *ACS Appl. Mater. Interfaces*, 2021, **13**, 29511-29521.

S11 M. A. Patel, F. Luo, M. R. Khoshi, E. Rabie, Q. Zhang, C. R. Flach, R. Mendelsohn, E. Garfunkel, M. Szostak and H. He, *ACS Nano*, 2016, **10**, 2305-2315.

S12 C. X. Li, M. M. Yang, R. H. Liu, F. F. Zhao, H. Huang, Y. Liu and Z. H. Kang,

RSC Adv., 2014, **4**, 22419-22424.

S13 Z. Long, L. Sun, W. Zhu, G. Chen, X. Wang and W. Sun, *Chem. Commun.*, 2018, **54**, 8991-8994.

S14 A. Villa, M. Schiavoni, P. F. Fulvio, S. M. Mahurin, S. Dai, R. T. Mayes, G. M. Veith and L. Prati, *J. Energy Chem.*, 2013, **22**, 305-311.

S15 J. Meng, Y. Z. Liu, Q. Q. Xia, S. Liu, Z. H. Tong, W. S. Chen, S. X. Liu, J. Li, S. Dou and H. P. Yu, *Small Methods*, 2021, **5**, 2100964.

S16 F. Yang, X. Fan, C. Wang, W. Yang, L. Hou, X. Xu, A. Feng, S. Dong, K. Chen, Y. Wang and Y. Li, *Carbon*, 2017, **121**, 443-451.

S17 K. C. Poon, W. Y. Wan, H. B. Su and H. Sato, *ACS Appl. Energy Mater.*, 2021, **4**, 5388-5391.

S18 Z. Bi, L. Huo, Q. Kong, F. Li, J. Chen, A. Ahmad, X. Wei, L. Xie and C.-M. Chen, *ACS Appl. Mater. Interfaces*, 2019, **11**, 11421-11430.

S19 F. Wu, R. Q. Dong, Y. Bai, Y. Li, G. H. Chen, Z. H. Wang and C. Wu, *ACS Appl. Mater. Interfaces*, 2018, **10**, 21335-21342.

S20 X. Zhou, X. Liu, F. Qi, H. Shi, Y. Zhang and P. Ma, *Sep. Purif. Technol.*, 2022, **292**, 120954.

S21 K. Gunasekaran Govindarasu, R. Venkatesan, M. Eswaran and P. Arumugam, *Adv. Powder Technol.*, 2022, **33**, 103439.

S22 H. Sun, C. Liu, D. Guo, S. Liang, W. Xie, S. Liu and Z. Li, *RSC Adv.*, 2022, **12**, 24724-24733.

S23 H. Zhang, S. Wang, H. Zhang, L. Cui and F. Cao, Fuel, 2022, 324, 124024.

S24 Y. Wei, W. Cheng, Y. Huang, Z. Liu, R. Sheng, X. Wang, D. Jia and X. Tang, *Langmuir*, 2022, **38**, 11610-11620.

S25 M. Zhou, Y. Xu, G. Luo, Q. Zhang, L. Du, X. Cui and Z. Li, *Chem. Eng. J.*, 2022, **432**, 134440.

S26 R. Wu, Y. P. Hang, J. H. Li and A. L. Bao, *Surf. Interface Anal.*, 2022, **54**, 881-891.

S27 G. R. Paixão, N. G. Camparotto, G. d. V. Brião, R. d. L. Oliveira, J. C. Colmenares, P. Prediger and M. G. A. Vieira, *Chem. Eng. Res. Des.*, 2022, **187**,

225-239.

S28 K. M. S. Khalil, W. A. Elhamdy and A. A. Elsamahy, *Colloid and Surface A*, 2022, **641**, 128553.